Subduction-induced upwelling of a hydrous transition zone: Implications for the Cenozoic magmatism in Northeast China

Lin Chen[1], Manuele Faccenda[2,*]

[1] State Key Laboratory of Lithospheric Evolution, Institute of Geology and Geophysics, Chinese Academy of Sciences, Beijing 100029, China

[2] Dipartimento di Geoscienze, Università di Padova, 35131 Padova, Italy

Corresponding author: Manuele Faccenda (manuele.faccenda@unipd.it)

Key Points:

- Subduction-induced upwelling of a hydrous TZ produces partial melting in the deep upper mantle
- This process could explain intracontinental magmatism in the overriding plate
- The water released by deep slab dehydration is absorbed by the TZ nominally anhydrous minerals

Abstract

The widespread Cenozoic basalts in northeast China are commonly thought to be related to the stagnation of the Pacific slab in the transition zone and its deep dehydration. By incorporating experimentally constrained phase diagrams of hydrous mantle and melting conditions at high pressures into 2-D petrological-thermomechanical models, here we model the interaction of a subducting slab with a hydrous transition zone (TZ) and examine its potential role in generating intracontinental magmatism. The model results show that descending of the oceanic slab first forces up the material in the TZ. Depending on the water content in the TZ, the upwelling hydrous material may undergo dehydration melting above the TZ. As a large slab stagnates within the TZ owing to the lower mantle resistance, the deep melting migrates progressively towards the overriding continent's interior, generating plutonic/volcanic rocks in the continental crust far away from the trench. The amount of deep melting and surface magmatism is obviously related to the amount of water stored in the TZ. In contrast, the water stored in the cold core of the subducting slab and released in the transition zone does not generate melting as it is entirely absorbed by mantle transition zone nominally anhydrous minerals. Comparing the model results with the distribution of the late Cenozoic basalts in northeast China, we suggest that the intracontinental magmatism there was likely caused by deep dehydration melting induced by the slab-transition zone interaction.

1 Introduction

Volcanism at plate boundaries can be understood well in the framework of plate tectonics, whereas the origins of the volcanism occurring within plate's interiors (intraplate volcanism) remain elusive. It is generally thought that intraplate volcanism is caused by mantle plumes originating from a hot thermal layer at the core-mantle boundary [*Morgan*, 1971]. However, some intraplate volcanism does not fit the mantle plume model. For example, Cenozoic basalts are widely distributed in northeast China, which is more than 1000 km away from the Japan trench (Figure 1). Because there is neither slow seismic anomaly in the lower mantle [*Montelli et al.*, 2004; *Zhao,* 2004], nor evidence for a flood basalt and hot-spot track associated with the impingement of a mantle plume [*Tang et al.*, 2014), mantle plume is unlikely the cause for the intraplate Cenozoic volcanism in northeast China.

Seismic tomography models show that low-velocity anomalies extend to the deep part of the upper mantle [*Zhao et al.*, 2004; *Lei and Zhao*, 2005] and subhorizontal high-velocity zones are present in the mantle transition zone (TZ) under northeast China [*Huang and Zhao*, 2006; Figure 1), indicating that the subducting Pacific slab is stagnant in the transition zone. [*Zhao and Ohtani*, 2009] proposed that the upper mantle above the stagnant slab under northeast China is part of a big mantle wedge (BMW), and suggested that the dehydration of the stagnant slab in the TZ and associated mantle upwelling in the BMW cause the intraplate volcanism in East Asia. Some researchers argued against the BMW model on the basis of the absence of any island-arc geochemical signature in the erupted basalts, and suggested that piling up and thickening of stagnant slab in the TZ drives upwelling of normal asthenosphere and leads to decompression melting at shallow depths [*Chen et al.*, 2007; *Zou et al.,* 2008]. Recent seismic studies based on a denser seismic array show that a continuous slow seismic anomaly extends from the TZ to the

surface beneath the Changbai volcano (the largest active volcano in NE China; [*Tang et al.,* 2014; *Guo et al.,* 2018], suggesting subduction-induced mantle upwelling. Although all these studies point to a link between the intraplate volcanism and slab-transition zone interaction, the origin and dynamics of mantle upwelling are still much enigmatic and debated.

The above-mentioned controversy in part arises from our incomplete understanding about the water distribution in Earth's mantle and its influence on mineral physical properties [e.g., *Ohtani et al.*, 2004; *Hirschmann*, 2006; *Karato*, 2011; *Faccenda*, 2014]. The TZ, sandwiched between the upper and lower mantle, has the capability of storing large amounts of water due to the presence of the nominally anhydrous minerals (NAMs) wadsleyite and ringwoodite (e.g., [*Ohtani et al.*, 2004; *Hirschmann*, 2006; *Pearson et al.*, 2014; *Fei et al.*, 2017]). A hydrous TZ has been suggested to play a key role in cratonic lithospheric thinning [*Windley et al.*, 2010; *Kusky et al.*, 2014] and intracontinental magmatism [*Wang et al.*, 2015], although such correlations remain enigmatic. It is also well established that even small amounts of water have significant effects on the mantle melting conditions [*Inoue*, 1994; *Hirschmann*, 2006] and rheological properties [*Mei and Kohlstedt*, 2000]. Therefore, to advance our understanding of the dynamics of slab-transition zone interaction, it is necessary to incorporate our current knowledge of the water distribution in Earth's interior into geodynamic models.

Previous numerical studies on slab-transition zone interaction mainly focused on the cause for slab stagnation above the 660 km discontinuity or its penetration in the lower mantle (see the review by [*Goes et al.*, 2017], and highlighted the roles of viscosity jump, phase changes and density jump between upper and lower mantle, trench mobility, and/or slab strength in shaping slab morphologies in the mantle [e.g., *Cizkova and Bina*, 2013; *Garel et al.*, 2014; *King et al.*, 2015]. A few numerical studies have paid attention to the high H_2O storage capacity of the TZ and

its role in modifying mantle flow and slab behavior during subduction [*Richard and Iwamori*, 2010; *Nakao et al.*, 2016; *Wang et al.*, 2016]. Nevertheless, the potential link between slab - hydrous transition zone interaction and terrestrial magmatism has not been systematically investigated.

Here we use 2-D petrological-thermomechanical models to investigate the effects of varying water distribution on the subduction dynamics by incorporating: (1) stability of hydrous phases in peridotite [*Iwamori*, 2004] and basalt [*Poli and Schmidt*, 2002], (2) water storage capacity of NAMs and wet solidi in peridotite at the whole upper mantle and TZ conditions [*Litasov*, 2011; *Litasov et al.*, 2014], and (3) peridotite melt density at high pressure [*Suzuki et al.*, 1998; *Suzuki and Ohtani*, 2003]. These factors are either not considered or oversimplified in previous studies [e.g., *Richard and Iwamori*, 2010; *He*, 2014; *Wang et al.*, 2016]. Our emphasis is on the interaction of a subducting oceanic plate with a hydrous TZ and its magmatic expression on the overriding continental plate. The simulations will demonstrate that water content in the TZ controls the magmatism volume and distribution in the upper plate. Finally, the model results will be applied to explain the mechanism for the intraplate Cenozoic magmatism in northeast China.

2 Numerical modeling approach

We use 2D petrological-thermomechanical code I2VIS [*Gerya and Yuen*, 2003] to investigate the interaction of subducting slab with TZ. The code solves the coupled mass, momentum and energy conservation equations on a Eulerian frame, subject to the boundary conditions described below, using the finite difference method and marker-in-cell technique. At each time-step, the model velocity field is used to advect the Lagrangian markers. In turn, the new distribution of the markers is used to update the physical properties at the Eulerian mesh by distance-weighted bilinear interpolation [*Gerya and Yuen*, 2003]. All materials deform according to a composite

rheological model, which accounts for plastic yielding at shallow depths and low temperatures, and dislocation creep at greater depths and temperatures (see Supplementary Information for details). We use a thermodynamic model to compute mineral assemblages and their physical properties, such as density and heat capacity [e.g., *Connolly*, 2005; *Gerya et al.*, 2006].

2.1 Model design

In order to simulate a large-scale slab stagnation in the TZ as observed beneath East China [*Huang and Zhao*, 2006; *Fukao and Obayashi*, 2013], the computational domain is set as a two-dimensional Cartesian box, 6000 km wide and 700 km deep (Figure 2). The whole domain is resolved with 1501×351 Eulerian nodes with a uniform resolution of 4×2 km^2. There are 21 million Lagrangian markers randomly distributed in the domain. This allows us to monitor the material deformation on a fine scale.

The initial model is made up of two types of plates: a continental plate on the left side and an oceanic plate on the right side. The continental plate is composed of a 36-km-thick crust (a 16-km-thick felsic upper crust and a 20-km-thick mafic lower crust) and a 94-km-thick lithospheric mantle, giving a total lithosphere thickness of 130 km. The oceanic plate is composed of a 7-km-thick crust (a 2-km-thick basaltic upper crust and a 5-km-thick gabbroic lower crust) and an 85-km-thick lithospheric mantle, giving a total lithosphere thickness of 92 km. A weak zone is placed at the continental right margin to initiate subduction (Figure 2). The initial continental geotherm linearly increases from 273 K at the model surface to 1603 K at the lithosphere base, while the initial temperature field for the oceanic plate is defined using the half-space cooling model with a slab age of 70 Ma and a diffusivity of 10^{-6} m^2/s. An adiabatic gradient of 0.5 ℃/km is used for the sub-lithosphere mantle. Mechanical boundary conditions are free slip on the top, no slip on the

bottom, and periodic side boundaries. The thermal boundary conditions are constant temperature (273 K) on the top, remote fixed temperature on the bottom [*Gerya et al.*, 2006], and periodic side boundaries. A convergence rate of 5.0 cm/yr is imposed at the distal end of the oceanic plate (x=5348 km) to drive the model evolution.

2.2 Hydration and dehydration processes

Water can be present as a free fluid phase in pores, as hydrogen or hydroxyls incorporated in NAMs, or structurally bonded in hydrous phases [*Faccenda*, 2014]. Throughout this paper, we use 'hydrous' to mean water in NAMs, and 'hydrated' to mean stable hydrous minerals such as serpentine.

At shallow depths, the pore water in sediments is expelled due to compaction. To formulate this process, we assume that the pore water content linearly decreases from 2 wt.% at the seafloor to 0 wt.% at 75 km depth [e.g., *Gerya and Meilick*, 2011]:

$$X_{H_2O(wt\%)} = (1 - 0.013\Delta y)X_{H_2O(p)} \quad (1)$$

where $X_{H_2O(p)} = 2$ wt% is the water content at the seafloor and Δy is depth below the seafloor in km (0-75 km).

Incorporation or release of water in the H_2O-saturated oceanic crust is computed with a thermodynamic model down to 300 km, below which a constant $X_{H_2O(wt\%)} = 0.1.$ is imposed for NAMs of the mafic crust (Katayama et al., 2003, GRL). For the mantle, we adopt the phase diagram of the H_2O-saturated peridotitic rocks by [*Iwamori*, 2004] (Figure 3). We account for heterogenous mantle serpentinization by downscaling the water contents in the original phase

diagram such that $X_{H_2O(wt\%)} = 2.0$ for hydrated mantle rocks at shallow depths, corresponding to about 30% serpentinization. The hydrogen solubility in mantle NAMs is estimated from the wet solidi [*Litasov*, 2011] which indicate the maximum water content at given P-T conditions before melting. For intermediate temperatures, hydrogen solubility is estimated by linearly interpolating the water content of the two adjacent solidi (see Text S3).

We assume that the oceanic crust forming the seafloor is uniformly hydrated ($X_{H_2O(wt\%)} = 1.0$), while the underlying lithospheric mantle becomes hydrothermally altered for sufficiently large amounts of brittle deformation related to the bending at the trench-outer rise system ($X_{H_2O(wt\%)} = 2.0$; [*Faccenda et al.*, 2008]). More in detail, lithospheric mantle hydration occurs when the plastic strain exceeds 0.01 and down to a maximum depth of 15 km below the Moho.

Upon subduction, temperature increases within the slab, such that water-bearing minerals decompose at a particular depth, releasing free aqueous fluids [*Gerya et al.*, 2006]. Similarly, with increasing temperature or decreasing pressure, the hydrogen solubility in NAMs decreases and excess free fluids are produced. In both cases, a new Lagrangian particle is generated which migrates according to the Darcyan velocity:

$$v_{x(water)} = v_x - koef\, \partial P_s/\partial x \qquad (2)$$

$$v_{y(water)} = v_y - koef\left(\partial P_s/\partial y - \rho_f g_y\right) \qquad (3)$$

where v_x and v_y are the local velocity of the solid mantle, P_s is the solid pressure, $\rho_f = 1000\ kg/m^3$ is fluid density, g_y the vertical component of acceleration of gravity, $koef = K/\phi\mu_f = 1.33 \cdot 10^{-13}\ m^3\ s/kg$, K and ϕ are the rock permeability and porosity, μ_f the fluid

viscosity. Once free water encounters a rock capable of incorporating water by hydration or wetting, moving water is consumed.

2.3 Partial melting and melt extraction

We assume that the melt fraction is a linear function of temperature (T) and pressure (P), and calculate the volumetric fraction of melting (M_0) for a given pressure and rock type using the following equation [e.g., *Gerya and Yuen*, 2003]:

$$M_0 = \begin{cases} 0, & T \le T_s \\ \frac{T - T_s}{T_l - T_s}, & T_s < T < T_l \\ 1, & T \ge T_l \end{cases} \qquad (4)$$

where $T_s(P, X_{H_2O})$ and $T_l(P)$ are the solidus and liquidus temperature of a given rock type, respectively. The dry/wet solidus and liquidus curves have been parametrized from [*Litasov*, 2011] according to the equations reported in Text S3. At a given pressure, melting temperatures for different water contents are computed by linear interpolation of the two adjacent wet solidi.

The effective density of partially molten rocks (ρ_{eff}) is calculated according to the relation:

$$\rho_{eff} = \rho_{solid} - M(\rho_{solid} - \rho_{molten}) \qquad (5)$$

where ρ_{solid} and ρ_{molten} are the densities of solid and molten rocks at given temperature and pressure. M is the total amount of melt after melt extraction, and its relationship with M_0 is given in Eq. (10).

The effect of latent heating from equilibrium melting or crystallization is included implicitly by varying the effective heat capacity (C_{pe}) and thermal expansion (α_e) of melting/crystallizing rocks:

$$C_{pe} = C_p + Q_L[(\partial M/\partial T)_{P=const}] \quad (6)$$

$$\alpha_e = \alpha + \rho Q_L[(\partial M/\partial P)_{T=cont}]/T \quad (7)$$

where C_p is the heat capacity of the solid rock, and Q_L is the latent heat of melting.

The effective viscosity of partially molten rocks (M>0.05) is calculated according to [e.g., *Katz et al.*, 2006]:

$$\eta_{melt} = \eta_{ductile} \exp[-28 * (M - 0.05)] \quad (8)$$

where $\eta_{ductile}$ is the pre-melt creep viscosity of the rocks, which depends on composition, pressure, temperature and strain rate (see Table S1 for details).

The solidi for the peridotite with varying water contents (i.e., the white lines in Fig. 3) are based on the compilation of [*Litasov*, 2011]. We adopt the empirical formula from [*Suzuki et al.*, 1998] and [*Suzuki and Ohtani*, 2003] to estimate density and thermal expansion for molten peridotitic rocks at high pressure.

$$\rho_{molten} = 2605 + 73.1 * P_{GPa} - 1.9 * P_{GPa}^2 + 2.916 * 10^{-2} * P_{GPa}^3 - 6 * 10^{-2} * (2633.15 - T) \quad (9)$$

where P_{GPa} is the pressure in GPa.

Melt extraction at depth and emplacement of plutonic and volcanic rocks at the surface occurs when the melt fraction exceeds a critical threshold (e.g., [*Sizova et al.*, 2010]; see below). In the modeling, we use markers to track the amount of extracted melt. The total amount of melt (M) for each marker is calculated as:

$$M = M_0 - \sum_n M_{ext} \quad (10)$$

where $\sum_n M_{ext}$ is the total melt fraction extracted during the previous n extraction episodes. Rocks are viewed as refractory when the extracted melt fraction is greater than the standard one (i.e., $\sum_n M_{ext} > M_0$). If the total amount of melt exceeds a pre-defined threshold, M_{min} (we use a reference $M_{min} = 5\%$ and test its effect on the generation of intracontinental magmatism), the melt fraction $M_{ext} = M - M_{min}$ is extracted and $\sum_n M_{ext}$ is updated. The water content in the residual mantle is scaled by a factor M_{min}/M, which increases its melting temperature. It is assumed that extracted melts are transmitted instantaneously to emplacement areas in the form of plutonic/volcanic rocks, as segregated magma migrates faster than rocks deform [e.g., *Hawkesworth et al.*, 1997].

3 Model results

We performed ten simulations to examine the effects of different water contents in the TZ (ranging from 0 to 0.5 wt%), slab age, convergence rate and M_{min} on slab-transition zone interaction and magmatism in the upper plate. For each simulation, we observe quite similar

geodynamic processes. Therefore, we first present the detailed model results from the reference model (0.3 wt% H_2O in the TZ), and then we will demonstrate how different key parameters may modulate the interaction of the subducting slab with the TZ and intracontinental magmatism. A summary of all the simulations is given in Table 1.

Table 1 Parameters and results of conducted simulations [a]

Model name	V_c (cm/a)	Water content in TZ (wt %)	M_{min} (%)	Slab age (Ma)	Intracontinental magmatism	Figures
Sta0	5.0	anhydrous	5	70	No	5, 7
Sta1	5.0	0.1	5	70	No	5
Sta2	5.0	0.2	5	70	Yes	5, 7
Sta3 (ref.)	5.0	0.3	5	70	Yes	1, 3-5, 7
Sta4	5.0	0.4	5	70	Yes	5
Sta5	5.0	0.5	5	70	Yes	5, 7
Sta6	5.0	0.3	1	70	Yes	6, 7
Sta7	5.0	0.3	5	40	Yes	7, S1
Sta8	2.5	0.3	5	70	Yes	7, S2
Sta9	5.0	0.3	2	70	Yes	7, S3

[a] V_c, convergence rate, and M_{min} is the minimum threshold of melt fraction for melt extraction.

3.1. Reference model with a 0.3 wt % TZ

The reference model ('Sta3' in Table 1) is characterized by a prescribed hydrous TZ with 0.3 wt% H_2O. Subduction initiates through bending and descending of the oceanic lithosphere along the preexisting weak zone. After 10.6 Myr of subduction, the oceanic lithosphere plunges into the upper mantle with a steep dip angle (Figure 4a). The subducted oceanic crust continuously dehydrates in depths ranging from 20 to 300 km, forming a thin highly hydrous layer atop the slab (Figure 4b). Meanwhile, a serpentinized layer (yellow material in Figure 4) forms beneath the oceanic crust due to the bending-related brittle deformation at the trench -outer rise system. Fluids released from the slab at shallow depths are expelled upward, generating partial melting and arc-volcanism in the overlying rock column and serpentinization within the upper plate forearc mantle. Deeper, the slab drives the upwelling of the hydrous TZ material in front of the slab. As a consequence, a hydrous melt emerges at the tip of the upwelling flow due to the change of the local melting conditions (see the solidus temperature shown in Figure 5).

After 19.3 Myr of subduction, the sinking slab reaches the base of the TZ, where it is sub-horizontally deflected due to the resistance of the bottom boundary and from the increase in density and viscosity resulting from the post-spinel transition (Figure 4c). At this stage, the interaction of the sinking slab with the TZ triggers more vigorous upwelling of the hydrated mantle and water content (Figure 4c, d). The upwelling material undergoes hydrous melting above ~400 km depth due to the lowering of solidus (Figure 5b), and the melting front arrives at ~200 km depth. This is accompanied by melt extraction, which leads to the emplacement of plutonic/volcanic rocks in the crust of the overriding continental lithosphere (see magenta material in Figure 4c). The emplacement of the plutonic/volcanic rocks is up to ~700 km away from the trench. We will

discuss the relationship between the intracontinental magmatism and water content in the TZ below.

At the mature stage of subduction (>38 Myr), the cold and strong subducting slab continuously tunnels the hydrous TZ, leading to a large-scale slab stagnation in the TZ (>1000 km in the horizontal direction; see Figure 4e). The stagnant slab evacuates large amounts of the hydrated mantle and water out of the TZ and results in extensive hydrous melting above ~400 km depth (Figure 4f and Figure 5c). The accompanied melt extraction produces more plutonic/volcanic rocks in the upper plate's crust, which extend up to ~900 km away from the trench.

3.2. Effects of the water content in the TZ

In this section, we investigate the correlation between the water content in the TZ and the extent of intracontinental magmatism by conducting a series of experiments, in which the water content in the TZ is systematically varied.

Figure 6 shows a comparison among the models with different water contents in the TZ. For comparison purposes, all the model snapshots are selected with an equivalent amount of subduction (i.e., ~38 Myr of subduction). It is clear that all the models exhibit similar slab stagnations in the TZ. The differences mainly lie in the following two aspects: (1) the amount and distribution of hydrous melt in the upper mantle; and (2) the amount of the plutonic/volcanic rock volume in the upper plate crust. The model with an anhydrous (Figure 6a) or lowly hydrous (0.1 wt%; Figure 6b) TZ predicts hydrous melting in the upper mantle and related arc-volcanism only in the region close to the trench. In contrast, the models with higher water contents in the TZ produce hydrous melting above the stagnant slab and broader distribution of magmatic rocks

within the overriding continental crust (Figure 6c-f). The amounts of hydrous melting and magmatic rocks depend obviously on the amount of water stored in the TZ. The more water the TZ holds, the larger the amounts of hydrous melt and associated plutonic/volcanic rocks are generated during the interaction of subducting slab with the TZ. For instance, when the water content in the TZ is up to 0.5 wt% ('Sta5' in Table 1), large portions of the hydrated TZ partially melts and the distribution of the resultant magmatic rocks in the upper plate can reach >1000 km away from the trench (Figure 6f). It should be noted that the results of this experiment are shown for the sake of the discussion as they reflect the evolution of an extreme case that is not representative of the Earth's mantle where little or no partial melting is observed.

3.3. Effects of slab age, convergence rate and M_{min}

Reducing the slab age ('Sta7', Fig. S1) and convergence rate ('Sta8', Fig. S2) essentially reduces the slab thermal parameter ($\Phi = \sin\delta v_{conv} t_{slab}$, where δ is the slab dip, v_{conv} the convergence rate and t_{slab} is the slab age), which translates in an increase of the slab mean temperature. As a consequence, slab dehydration reactions occur at shallower depths and closer to the trench. This is visible mainly in the forearc where large serpentinized plumes form due to the shallow crust dehydration, but also in a larger arc-magmatism in the model with a slower convergence rate. In the model with a younger oceanic plate, the slab dip is lower so that most of the fluids are released in the forearc region and a lower volume of arc-magmatism is observed.

We have also tested the amount and distribution of extracted magmatic rocks when using a lower minimum threshold for melt extraction M_{min} ('Sta6', Fig. 7; 'Sta9', Fig. S3). This is justified by the experimental evidence that pore interconnectivity and subsequent melt migration could be achieved at very low melt fractions [e.g., *Laumonier et al.*, 2017]. Decreasing M_{min} from

5% ('Sta3') to 1% ('Sta6') leads to an obvious increase in the overall volume of volcanic and plutonic magmatic rocks and a progressive migration of the magmatism toward the continental interior (Fig. 7, S3).

3.4. Intracontinental magmatism

To illustrate the relationship between the water content in the TZ and intracontinental magmatism, we compare the distribution of magmatic rock volumes resulted from the models with different water contents in TZ after about 1950 km of subduction (Figure 8a). All the models except 'Sta0', which has an anhydrous TZ, exhibit a bimodal-type distribution of magmatic rocks. The primary peak is associated with arc-volcanism and we refer to it as subduction zone arc-magmatism. The second peak is relatively smaller and situated in the intracontinental setting (>500 km away from the trench). As we have illustrated above, its generation is associated with hydrous melting triggered by the slab-transition zone interaction. In comparison, we refer to the second one as intracontinental magmatism. According to our models, a prerequisite for generating intracontinental magmatism during slab-transition zone interaction is that the TZ should hold a considerable amount of water ($\geq$ 0.2 wt%). The interaction of an anhydrous or lowly hydrous TZ with a descending slab produces no hydrous melting in the upper mantle and thus no intracontinental magmatism in the overriding continent. In addition, as the water content in the TZ increases or M_{min} is reduced, the volume of intracontinental magmatism increases and the distribution of volcanic/plutonic rocks migrates progressively towards the continental interior (Figure 8b). The convergence rate or slab age has no significant influence on the generation of the intraplate volcanism.

3.5. Fate of the water stored in the slab mantle

The water that is still present in the slab past the volcanic arc (mainly within the sub-Moho mantle) is transported down to the TZ either by the formation of Dense Hydrous Magnesium Silicate (DHMS) phases or, when dehydration reactions occur, due to unbending-related stresses which favor water migration slab-inward and wetting of the slab NAMs [e.g., *Faccenda and Mancktelow*, 2010; *Faccenda et al.*, 2012].

The hydrous minerals within the sub-Moho mantle decompose entirely in the TZ due to the increasing temperature, generating TZ NAMs and free fluids. However, in our models the released water does not generate any partial melting as it is entirely absorbed by the relatively cold TZ NAMs within or nearby the stagnating slab. As a consequence, a thin wet TZ layer characterized by high hydrogen solubility forms above the slab (see inset in Fig. 4e). Hence, differently from what is commonly envisaged, the fluids generated from the decomposition of DHMS phases in the TZ should not readily generate intracontinental magmatism, but they should rather contribute to rehydrate this mantle level. Upon TZ mantle thermal relaxation occurring over the following several Myrs, this water could then be gradually released (because of the decreasing hydrogen solubility with increasing temperature or of the decomposition of Al-rich hydrous phases) and redistributed over a larger, metasomatized mantle portion and/or eventually induce partial melting within the TZ. Upon slab avalanching, such a metasomatized mantle portion would sink into the lower mantle and experience partial melting given the low hydrogen solubility of lower mantle minerals. It is important to notice that the employed petrological model ignores the potential rehydration of the oceanic crust where Al-rich hydrous phases could stabilize at those P-T conditions [e.g., *Pamato et al.*, 2015], thus absorbing most of the released water.

4 Discussion

4.1. Water distribution in the TZ

The main assumption in the simulations presented in this study is that water is present in the TZ before the beginning of the subduction event associated with intraplate volcanism. Water can be delivered to the TZ by, for example, previous episodes of subduction of relatively cold plates, where DHMS phases are stable to great depths. Dehydration of slabs stagnating in the TZ would rehydrate this mantle level where olivine polymorphs can host up to 2-3 wt. % H2O at relatively low temperatures [e.g., *Litasov et al.,* 2011]. For large water contents (> 1 wt. %; [*Mao et al., 2008]*), seismic velocity are significantly reduced and such a wet thin layer could explain the negative reflectors identified by receiver function studies in proximity of the Pacific slab below the Japan Sea and of the Juan de Fuca Plate stagnating beneath Western U.S. [*Tauzin et al., 2017*]. These volatiles reside in the TZ until the next subduction episode causing TZ upwelling and magmatism at upper mantle depths. During its ascent, magma interacts with the solid matrix, possibly becoming more enriched in volatiles and incompatible elements. Accordingly, the intraplate volcanism might display a geochemical signature typical of dehydrating slabs. This mechanism is consistent with hydrogen enrichment on melt inclusions recently found in magnesium-rich olivine in from komatiitic lavas that implies a deep hydrous mantle reservoir fueled by subduction of a seawater-altered oceanic lithosphere [*Sobolev et al.*, 2019]. Alternatively, delamination of wet lithospheric roots in old suture zone that will tend to stagnate in the TZ can also contribute to increase the water content at these depths [*Green et al.*, 2010]. The water concentrations tested in the transition zone are consistent with the high electrical conductivity measured for example beneath the Philippine Sea [*Fukao et al.*, 2004], which is explained with 300-4000 wt ppm H2O [*Hae et al.*, 2006], or throughout the Pacific [*Utada et al.*,

2003], which implies an average content of 0.1-0.2 wt % in the Pacific mid mantle [*Huang et al.*, 2005]. The assumption of a homogeneously hydrated TZ obviously yields upper bound estimates of magmatism, and it was chosen just to simplify the model and to see where potentially anorogenic magmatism can be generated provided water is present in the TZ. We envisage that in nature water is likely to be heterogeneously distributed in the TZ and the amount of intraplate volcanism is lower than here estimated.

4.2. Implications for the Cenozoic magmatism in northeast China

Cenozoic intracontinental magmatism is widespread in Northeast China [*Zhou and Armstrong*, 1982; *Peng et al.*, 1986; *Miyashiro et al.*, 1986] with over 590 volcanic edifices and ~50,000 km^2 of basaltic lavas exposed (Liu et al., 2001). The Cenozoic volcanic rocks were mostly formed after 20 Myr [*Peng et al.*, 1986], and consist mainly of basanite, alkali olivine basalt, and tholeiite, with minor evolved trachyte and alkaline to peralkaline rhyolite [*Chen et al.*, 2007]. Ultramafic xenoliths, mainly spinel lherzolite and harzburgite, are common in basanite and alkali basalt [*Fan and Hooper*, 1989]. The Changbai basalts first erupted in the Early Miocene and continue to the present with several interruptions [*Liu*, 1999]. The last eruption age at Tianchi (the youngest volcano in the Changbai volcanic field) is about 1000 years ago [*Wei et al.*, 2007, 2013]. Chifeng basalts were mainly erupted between 23.8 and 6.1 Myr, which forms 100-450-m thick sheet-like lava flows covering an area of ~3000 km^2 and becomes younger westward [*Han et al.*, 1999; *Wang et al.*, 2015]. The occurrence of these Cenozoic basalts is over 1000 km away from the Japan trench, and lies above the stagnant Pacific slab (Figure 1; [*Zhao et al.*, 2004; *Huang and Zhao*, 2006]). Slow P-wave anomalies lie beneath the Changbai and Chifeng volcanic fields (Fig. 1b), although below the latter the P-wave anomaly appears to be deeper and smaller in magnitude

possibly because of (i) the extinguished volcanic phase in the area and/or (ii) the incomplete and heterogeneous sampling of the medium of P-waves that could affect the resolution ad could generate artefacts in presence of seismic anisotropy [*Bezada et al.*, 2016]. The intracontinental magmatism has been attributed to either shallow processes, such as continental rifting [e.g., *Liu et al.*, 2001] and decompression melting during asthenospheric upwelling induced by slab subduction or stagnation [e.g., *Chen et al.*, 2007; *Zou et al.*, 2008; *Zhao et al.*, 2009], or to deep processes, such as (i) wet and cold mantle plumes originated from dehydration of the stagnant Pacific slab [e.g., *Richard and Iwamori*, 2010; *Zhao and Ohtani*, 2009] and/or from instabilities in the hydrous TZ [e.g., *Wang et al.*, 2015], and (ii) deep hot mantle upwelling induced by the Pacific plate subduction [e.g., *Faccenna et al.*, 2010]. A recent compilation of water contents in the Cenozoic alkali basalts and peridotite xenoliths from eastern China indicates that the Cenozoic basalts were likely sourced from the TZ, instead of from the lithospheric mantle [*Xia et al.*, 2017]. However, while some geochemical studies highlight the role of the subducted crust in the mantle source of this volcanism [*Sakuyama et al.*,2013; *Guo et al.*, 2016], others indicate that volcanic rocks and associated mantle xenoliths in NE China are rich in alkaline and incompatible trace elements, and have significant ^{230}Th excesses and low U/Th ratios, arguing against a significant influence of the fluids released from the subducted Pacific slab [*Chen et al.*, 2007; *Zou et al.*, 2008]. In particular, the Changbai basalts are characterized by high Ba/Th and ^{207}Pb/^{206}Pb ratios and an EM1-like (enriched mantle-1) isotopic signature, which led [*Kuritani et al.*, 2011] to suggest that these geochemical features record an ancient hydration event in the transition zone occurred more than 1 Gyr ago, probably as a result of dehydration of an ancient subducted slab. Similarly, the Wudalianchi basalts are characterized by K_2O enrichment and an EM1-like isotopic signature [*Kuritani et al.*, 2013], which was again interpreted as caused by an upwelling of a hydrous mantle

plume originated from the TZ that was hydrated through the stagnation of the ancient subducted slab and the recent Pacific slab. The ancient hydration event, combined with a recent hydration event associated with dehydration of the subducted Pacific slab, can lead to a remarkably hydrous TZ beneath eastern China consistent with the observed high electrical conductivity [*Karato*, 2011].

Our model results demonstrate that the interaction between the subducting slab and the hydrous TZ can cause the upwelling of the wet TZ. The resulting stagnant slab forces up the water-bearing minerals in the TZ and triggers dehydration melting above the TZ owing to low water storage capacity of the upper mantle minerals. Such hydrous melting in the deep upper mantle and associated magmatism can occur far from the trench. Figure 9 shows the evolution of the intraplate magmatic rocks through time. The presence of intraplate magmatism occurs after 10-15 Myr of subduction initiation. For a moderately hydrous TZ (0.3 wt; see the dark green curve in Fig. 9), the cumulative volume of the intraplate magmatic rocks increases fast in the first 10 Myr, and then gradually becomes steady. A recent plate reconstruction study based on a high-resolution model of P-wave tomography and paleo-age data of ancient seafloor shows that the stagnant Pacific slab beneath East China has been in the TZ for no more than ~10-20 million years [*Liu et al.*, 2017]. The young ages for the stagnant Pacific slab are in agreement with the eruption ages of the Cenozoic basalts in NE China and our model results. By assuming an average subduction of 7 cm/yr (e.g., [*Liu et al.*, 2017]), we estimate the time for the slab reaching the 660-km discontinuity to be 9.4 Myr since subduction. This is consistent with the estimation by [*Liu et al.*, 2017]. We conclude that the subduction-induced upwelling of a hydrous can explain the generation of the late Cenozoic basalts in northeastern China.

4.3. Model limitations

Our models focus on the interaction of subducting slabs with the TZ and the potential magmatic expressions and capture some key processes, such as the presence of water in the upper mantle and TZ, hydration/dehydration reactions, hydrous melting. They have been simplified in some other aspects, which will be discussed below.

Limited vertical dimension. The vertical dimension of all the models is confined to a depth of 700 km. This allows us to have a high spatial resolution to examine the subduction dynamics in the upper mantle and TZ. Extension of the model depth to a greater depth (e.g., 1000 km), which is not presented here, demonstrates that the dip angle of the subducting slab is smaller, the stagnant slab in the TZ is more deflected, and the distribution of the intracontinental magmatism is more diffuse when compared to the presented model with a 700-km bottom. However, the basic results from the presented models, such as deep dehydration melting and occurrence of intracontinental magmatism, still hold.

Limited amount of trench retreat. The subductions in all the models are driven by a prescribed convergence at the distal end of the oceanic plate, which allows to control the slab thermal age at depth. This is different from the free-subduction models [e.g., *Cizkova and Bina*, 2013; *Garel et al.*, 2014; *King et al.*, 2015], which have a mobile trench and favor trench retreat. Goes et al. (2017) indicated that older and stronger oceanic plates are more capable of resulting in trench retreat, and trench retreat facilitates slab flattening in the TZ. Models with dynamical trench motion show that variable trench mobility controlled by slab internal and external forcing is the most likely cause for various modes of subduction-transition zone interaction [e.g., *Cizkova and Bina*, 2013; *Garel et al.*, 2014]. It is reasonable to believe that the stagnant slab will extend over a larger distance and the associated intracontinental magmatism will be farther away from the trench if trench retreat is

included in our models. Furthermore, trench retreat would facilitate the formation of a back-arc basin, simulating the formation of the Japan Sea.

Melt extraction. In our model, melt segregates from the residual mantle when the melt fraction exceeds the pre-defined threshold M_{min}, and it is then extracted directly at the surface neglecting important petrological and thermo-mechanical interactions with the porous matrix. In nature, melt migration to the surface occurs via reactive porous flow, whereby the melt and porous matrix compositions continuously change through a series of petrological reactions [for example, *Kelemen et al.*, 1995; *Rampone et al.*, 2004]. In order to simulate such an interaction, a thermodynamic melting model is necessary. However, due to technical limitations of the laboratory experiments at extreme P-T conditions, existing thermodynamic melting models [e.g., *Ghiorso et al.*, 2002; *Jennings and Holland*, 2015] have been calibrated to depths ≤ 150 km. For this reason, we have chosen to not model reactive porous flow in such a petrological system that is poorly constrained at high pressures typical of the lowermost upper mantle. It is important to highlight that magma rising paths can be deflected from the vertical direction assumed here by additional flow and pressure components generated in a strongly deforming porous matrix [*Butler*, 2009]. Nevertheless, for typical upper mantle conditions, buoyance forces are larger than matrix shear-induced forces, and rising porous waves should not deviate much from the vertical direction.

The role of CO_2. The release of water alone from dehydrating stagnant slabs can hardly produce wet plumes and anorogenic volcanism as the water is absorbed by the thick mantle bearing NAMs with high hydrogen solubility. However, it has been suggested that the release of both H_2O and CO_2 from the sediments, crust and serpentinized mantle could locally generate particular redox conditions and low melting temperatures which would led to volatile-bearing plumes upwelling from the TZ to the Lithosphere – Asthenosphere boundary [*Safonova et al.*, 2015]. This mechanism

represent an alternative explanation to the intraplate volcanism that is in line with the BMW hypothesis, and that deserves to be tested in the next generation of numerical simulations accounting for the presence of a larger number of volatile species other than only water. Here we note that pre-existence in the TZ of both water absorbed by NAMs and carbon precipitated through redox-freezing reactions [*Sun and Dasgupta*, 2019], which were eventually released by an old subduction event and did not interact sufficiently to be mobilized, could also explain the formation of anorogenic volcanism with the mechanism proposed in this study, i.e., by the upwelling of the metasomatized, volatile-bearing TZ induced by the latest subduction episode.

5 Conclusions

In this study, we investigate the interaction of subducting slab with a hydrous TZ and its potential role in generating intracontinental magmatism by incorporating the hydrous phase relations and melting conditions at high pressures into 2-D petrological-thermomechanical models. The main findings are as follows.

1. The descending of the oceanic slab forces up the hydrous mantle in the TZ and induces dehydration melting in the deep upper mantle. As the slab stagnates in the TZ, the deep dehydration melting progressively migrates towards the continental interior, generating plutonic/volcanic rocks in the overriding continental crust.

2. The amounts of deep dehydration melting and associated magmatic rocks depend on the water content hosted in the TZ. Our models demonstrate that deep hydrous melting and associated surface magmatism can be formed only by the interaction of subducting slab with a markedly hydrous (≥0.2 wt%) TZ. The results hold also in the more realistic case of a heterogeneously hydrous TZ.

3. Fluids released in the TZ by DHMS phases decomposition are entirely absorbed by the relatively cold TZ NAMs within and above the slab. Because of the relatively low temperature within the slab, no partial melting is produced during the subduction timescale. Hence, deep dehydration of the Pacific plate likely does not contribute to the Cenozoic intracontinental magmatism in northeastern China.

4. Subduction-induced upwelling and dehydration melting in the deep upper mantle provides an alternative explanation for the intracontinental magmatism in northeast China.

Acknowledgments

We thank Taras Gerya for providing the I2VIS code, and Qin Wang, Zhu Mao and Juan Li for discussions. Zhiyong Yan helped plot Figure 1. All the figures were generated with GMT (https://www.soest.hawaii.edu/gmt/). This study is supported by the Strategic Priority Research Program (B) of the Chinese Academy of Sciences (XDB18030105), by the National Key Research and Development Project (2016YFC0600406) to LC, and by the ERC-StG NEWTON #758199 to MF. We are grateful to Valentina Magni and Jeroen van Hunen for their constructive comments. All the simulations were run on the TianHe-1A cluster at National Supercomputer Center in Tianjin and the Galileo/Marconi cluster at CINECA in Bologna. The data supporting the conclusions can be provided by the authors upon request.

References

1. Bercovici, D., Karato, S., 2003. Whole mantle convection and transition-zone water filter. Nature 425, 39–44.
2. Bezada, M., Faccenda, M., Toomey, D.R., 2016. Representing anisotropic subduction

zones with isotropic velocity models: A characterization of the problem and some steps on a possible path forward. Geochem. Geophys. Geosys., 17, 8, 3164-3189.

3. Butler, S.L., 2009. The effects of buoyancy on shear-induced melt bands in a compacting porous medium. Phys. Earth Planet. Int. 173 (1-2), 51-59.
4. Chen, Y., Zhang, Y., Graham, D., Su, S., Deng, J., 2007. Geochemistry of Cenozoic basalts and mantle xenoliths in Northeast China. Lithos 96, 108-126.
5. Cížková, H., Bina, C.R., 2013. Effects of mantle and subduction-interface rheologies on slab stagnation and trench rollback. Earth Planet. Sci. Lett.379, 95–103.
6. Connolly, J.A.D., 2005. Computation of phase equilibria by linear programming: a tool for geodynamic modeling and its application to subduction zone decarbonation. Earth Planet. Sci. Lett. 236, 524–541.
7. Faccenda, M., Burlini, L., Gerya, T.V., Mainprice, D., 2008. Fault-induced seismic anisotropy by hydration in subducting oceanic plates. Nature 455, 1097–1100.
8. Faccenda, M., Gerya, T.V., Burlini, L., 2009. Deep slab hydration induced by bending-related variations in tectonic pressure. Nat. Geosci. 2, 790–793.
9. Faccenda, M. and Mancktelow, N. S., 2010. Fluid flow during unbending: implications for slab hydration, intermediate-depth earthquakes and deep fluid subduction. Tectonophys. 494, 149-154
10. Faccenda M., Gerya, T. V., Mancktelow, N. S. and Moresi, L., 2012. Fluid flow during slab unbending and dehydration: Implications for intermediate-depth seismicity, slab weakening and deep water recycling. Geochem. Geophys. Geosyst., 13, Q01010, doi:10.1029/2011GC003860.
11. Faccenda, M., 2014. Water in the slab: a trilogy. Tectonophysics 64, 1–30.

12. Faccenna, C., Becker, T.W., Lallemand, S., Lagabrielle, Y., Funiciello, F., Piromallo, C., 2010. Subduction-triggered magmatic pulses: A new class of plumes. Earth Planet. Sci. Lett. 299, 54-68.
13. Fei, H., Yamazaki, D., Sakurai, M., Miyajima, N., Ohfuji, H., Katsura, T., Yamamota, T., 2017. A nearly water-saturated mantle transition zone inferred from mineral viscosity. Sci. Adv. 3, e1603024.
14. Fan, Q.C., P.R. Hooper (1989), The mineral chemistry of ultramafic xenoliths of Eastern China: implications for upper mantle composition and the Paleogeotherms, Journal of Petrology, 30, 1117–1158.
15. Fukao, Y., Koyama, T., Pbayashi, M., Utada, H., 2004. Trans-Pacific temperature field in the mantle transition region derived from seismic and electromagnetic tomography. Earth Plant. Sci. Lett. 217, 425-434.
16. Fukao, Y., Obayashi, M., Nakakuki, T., 2009. Stagnant slab: a review. Annu. Rev. Earth Planet. Sci. 37, 19–46.
17. Garel, F., Goes, S., Davies, D.R., Davies, J.H., Kramer, S.C., Wilson, C.R., 2014. Interaction of subducted slabs with the mantle transition-zone: a regime diagram from 2-D thermo-mechanical models with a mobile trench and an overriding plate. Geochem. Geophys. Geosyst.15, 1739–1765.
18. Gerya, T.V., Yuen, D.A., 2003. Characteristics-based marker-in-cell method with conservative finite-differences schemes for modeling geological flows with strongly variable transport properties. Phys. Earth Planet. Inter. 140 (4), 293–318.
19. Gerya, T.V., Connolly, J.A.D., Yuen, D.A., Gorczyk, W., Capel, A.M., 2006. Seismic implications of mantle wedge plumes. Phys. Earth Planet. Inter. 156, 59–74.

20. Gerya, T.V., Meilick, F.I., 2011. Geodynamic regimes of subduction under an active margin: effects of rheological weakening by fluids and melts. J. Metamorph. Geol. 29, 7–31.
21. Ghiorso, M.S., Hirschmann, M.M., Reiners, P.W., Kress, V.C., 2002. The pMELTS: A revision of MELTS for improved calculation of phase relations and major element partitioning related to partial melting of the mantle to 3 GPa. Geochem., Geophys. Geosys. 3, 1–35. https://doi.org/10.1029/2001GC000217
22. Goes, S., Agrusta, R., van Hunen, J., and Garel, F., 2017, Subduction-transition zone interaction: A review. Geosphere 13, no. 3, 644–664, doi:10.1130/GES01476.1.
23. Green, H. W., Chen, W. P., Brudzinski, M.R, 2010. Seismic evidence of negligible water carried below 400-km depth in subducting lithosphere. Nature 467, 828-831.
24. Grove, T.L., Till, C.B., Krawczynski, M.J., 2012. The role of H2O in subduction zone magmatism. Annu. Rev. Earth Planet. Sci. 2012. 40:413–39.
25. Hae, R., Ohtani, E., Kubo, T., Koyama, T., Utada, H., 2006. Hydrogen diffusivity in wasdleyite and water distribution in the mantle transition zone. Earth Planet. Sci. Lett. 243, 141-148.
26. Han, B.-F., S.-G. Wang, and H. Kagami (1999), Trace element and Nd-Sr isotope constraints on origin of the Chifeng flood basalts, North China, Chemical Geology, 155, 187-199.
27. Hawkesworth, C.J., Turner, S.P., McDermott, F., Peate, D.W., van Calsteren, P., 1997. U–Th isotopes in arc magmas: implications for element transfer from the subducted crust. Science 276 (5312), 551–555.

28. He, L., 2014. Numerical modeling of convective erosion and peridotite-melt interaction in big mantle wedge: implications for the destruction of the North China Craton. J. Geophys. Res. Solid Earth 119, 3662–3677.
29. Hirschmann, M.M., 2006. Water, melting, and the deep Earth H2O cycle. Annu. Rev. Earth Planet. Sci. 34, 629–653.
30. Huang, X., Xu, Y., Karato, S.-I., 2005. Water content of the mantle transition zone from the electrical conductivity of wadsleyite and ringwoodite. Nature 434, 746-749.
31. Huang, J., D. Zhao (2006), High-resolution mantle tomography of China and surrounding regions, J. Geophys. Res., 111, B09305, doi:10.1029/2005JB004066.
32. Iwamori, H., 2004. Phase relations of peridotites under H2O-saturated conditions and ability of subducting plates for transportation of H2O. Earth Planet. Sci. Lett. 227, 57–71.
33. Inoue, T., 1994. Effect of water on melting phase relations and melt composition in the system Mg2SiO4–MgSiO3–H2O up to 15 GPa. Phys. Earth Planet. Inter. 85, 237–263.
34. Iwamori, H., 2004. Phase relations of peridotites under H_2O-saturated conditions and ability of subducting plates for transportation of H_2O. Earth Planet. Sci. Lett., 227, 57-71.
35. Iwamori, H., 2007. Transportation of H2O beneath the Japan arcs and its implications for global water circulation. Chem. Geol. 239, 182–198.
36. Jennings, E. S., Holland, T.J.B., 2015. A simple thermodynamic model for melting of peridotite in the system NCFMASOCr. J. Petrol. 56 (5), 869-892. https://doi.org/10.1093/petrology/egv020
37. Karato, S., 2011. Water distribution across the mantle transition zone and its implications for global material circulation. Earth Planet. Sci. Lett. 301, 413-423.
38. Katayama, I., Hirose, K., Yurimoto, H., Nakashima, S., 2003. Water solubility in majoritic

garnet in subducting oceanic crust. Geophys. Res. Lett. 30 (22), doi:10..1029/2003GL018127.

39. Kelemen, P.B., Shimizu, N., Salters, V.J.M., 1995. Extraction of mid-ocean ridge basalt from the upwelling mantle by focused flow of melt in dunite channels. Nature 375, 747-753.
40. King, S.D., Frost, D.J., Rubie, D.C., 2015. Why cold slabs stagnate in the transition zone. Geology 43, 231–234.
41. Kuritani, T., Ohtani, E., Kimura, J.-I., 2011. Intensive hydration of the mantle transition zone beneath China caused by ancient slab stagnation. Nat. Geosci. 4, 713–716.
42. Kuritani, T., Kimura, J.-I., Ohtani, E., Miyamoto, H., Furuyama, K., 2013. Transition zone origin of potassic basalts from Wudalianchi volcano, northeast China. Lithos, 156-159, 1-12.
43. Kusky, T.M., Windley, B.F., Wang, L., Wang, Z., Li, X., Zhu, P., 2014. Flat slab subduction, trench suction, and craton destruction: comparison of the North China, Wyoming, and Brazilian cratons. Tectonophysics 630, 208–221.
44. Laumonier,M., Farla, R., Frost, D.J., Katsura, T., Marquardt, K, Bouvier, A.-S., Baumgartner, L. P. 2017. Experimental determination of melt interconnectivity and electrical conductivity in the upper mantle. Earth Planet. Sci. Lett., 463, 286-297.
45. Litasov, K.D., 2011. Physicochemical conditions for melting in the Earth's mantle containing a C-O-H fluid (from experimental data). Russian Geology and Geophysics 52, 475-492.
46. Litasov, K.D., Shatskiy, A., Ohtani, E., Katsura, T., 2011. Systematic study of hydrogen incorporation into Fe-free wadsleyite. Phys. Chem. Min. 38, 75-84.

47. Litasov, K.D., Shatskiy, A., Ohtani, E., 2014. Melting and subsolidus phase relations in peridotite and eclogite systems with reduced C-O-H fluid at 3-16 GPa. Earth Planet. Sci. Lett. 391, 87-99.

48. Liu, J.Q. (1999), ChineseVolcanos. Science Press, Beijing. (in Chinese).

49. Liu, J., Han, J., Fyfe, W., 2001. Cenozoic episodic volcanism and continental rifting in northeast China and possible link to Japan sea development as revealed from K-Ar geochronology. Tectonophysics 339 (3–4), 385–401.

50. Liu, X., D. Zhao, S. Li, and W. Wei (2017), Age of the subducting Pacific slab beneath East Asia and its geodynamic implications, Earth Planet. Sci. Lett., 464, 166-174.

51. Mao, Z., Jacobsen, S.D., Jiang, F., Smyth, J.R., Holl, C.M., Duffy, T.S., 2008. Elasticity of hydrous wadsleyite to 12 GPa: implications for Earth's transition zone. Geophys. Res. Lett. 35 (2), https://doi.org/10.1029/2008GL0356618.

52. Mei, S., Kohlstedt, D.L., 2000. Influence of water on plastic deformation of olivine aggregates, 2. Dislocation creep regime. J. Geophys. Res. 105, 21471–21481.

53. Miyashiro, A., 1986. Hot region and the origin of marginal basins in the western pacific. Tectonophysics 122 (3–4), 195–216.

54. Nakao, A., Iwamori, H., Nakakuki, T., 2016. Effects of water transportation on subduction dynamics: roles of viscosity and density reduction. Earth Planet. Sci. Lett. 454, 178–191.

55. Ohtani, E., Litasov, K., Hosoya, T., Kubo, T., Kondo, T., 2004. Water transport into the deep mantle and formation of a hydrous transition zone. Phys. Earth Planet. Inter. 143, 255–269.

56. Ohtani, E., and D. Zhao (2009), The role of water in the deep upper mantle and transition zone: dehydration of stagnant slabs and its effects on the big mantle wedge, Russian

Geology and Geophysics, 50, 1073-1078.

57. Pamato, M.G., Myhill, R., Boffa Ballaran, T., Frost, D.J., Heidelbach, F., Miyajima, N., 2015. Lower-mantle water reservoir implied by the extreme stability of a hydrous aluminosilicate. Nat. Geosci. 8, 75-79. https://doi.org/10.1038/ngeo2306.
58. Pearson et al., 2014. Hydrous mantle transition zone indicated by ringwoodite included with diamond. Nature 507, 221-224, doi:10.1038/nature13080.
59. Peng, Z.C., R.E. Zartman, K. Futa, and D.G. Chen (1986), Pb-, Sr- and Nd-isotopic systematics and chemical characterstics of Cenozoic basalts, eastern China, Chemical Geology, 59, 3-33.
60. Poli S and Schmidt MW (2002) Petrology of subducted slabs. Annu. Rev. Earth Planet. Sci. 30: 207–235.
61. Rampone, E., Romairone, A., Hofmann, A.W., 2004. Contrasting bulk and mineral chemistry in depleted mantle peridotites: evidence for reactive porous flow. Earth Planet. Sci. Lett. 218 (3-4), 491-506.
62. Richard, G.C., Iwamori, H., 2010. Stagnant slab, wet plumes and Cenozoic volcanism in East Asia. Phys. Earth Planet. Inter. 183, 280–287.
63. Safanova, I., Litasov, K., Maruyama, S., 2015. Triggers and sources of volatile-bearing plumes in the mantle transition zone. Geosci. Front. 6, 5, 679-685.
64. Sobolev, A.V., et al., 2019. Deep hydrous mantle reservoir provides evidence for crustal recycling before 3.3 billion years ago. Nature 571, 555-559.
65. Sun, C., Dasgupta, R., 2019. Slab-mantle interaction, carbon transport, and kimberlite generation in the deep upper mantle. Earth Planet. Sci. Lett. 506, 38-52.
66. Suzuki, A., Ohtani, E., Kato, T., 1998. Density and thermal expansion of a peridotite melt

at high pressure. Phys. Earth Planet. Inter. 107, 53–61.

67. Suzuki, A., Ohtani, E., 2003. Density of peridotite melts at high pressure. Phys Chem Minerals 30, 449-456.
68. Tang, Y., Obayashi, M., Niu, F., Grand, S.P., Chen, Y.J., Kawakatsu, H., Tanaka, S., Ning, J., Ni, J.F., 2014. Changbaishan volcanism in northeast China linked to subduction-induced mantle upwelling. Nat. Geosci.7 (6), 470–475.
69. Tauzin, B., Kim, S., Kennett, B.L.N., 2017. Pervasive seismic low-velocity zones within stagnant plates in the mantle transition zone: Thermal or compositional origin? Earth Planet. Sci. Lett. 477, 1-13.
70. Utada, H., Koyama, T., Shimizu, H., Chave, A.D., 2003. A semi-global reference model for electrical conductivity in the mid-mantle beneath the north Pacific region. Geophys. Res. Lett. 30 (4), doi:10.1029/2002GL016092.
71. Wang, X.-C., Wilde, S.A., Li, Q.-L., Yang, Y.-N., 2015. Continental flood basalts derived from the hydrous mantle transition zone. Nat. Commun. 6: 7700, doi: 10.1038/ncomms8700.
72. Wang, Y., Pavlis, G.L., Li, M., 2019. Heterogeneous distribution of water in the mantle transition zone inferred from wavefield imaging. Earth and Planetary Science Letters 505, 42-50.
73. Wang, Z., Kusky, T.M., Capitanio, F.A., 2016. Lithosphere thinning induced by slab penetration into a hydrous mantle transition zone. Geophys. Res. Lett., 43, 11,567–11,577, doi:10.1002/2016GL071186.
74. Wei, H., Y. Wang, J. Jin, L. Gao, S.-H. Yun, and B. Jin (2007), Timescale and evolution of the intracontinental Tianchi volcanic shield and ignimbrite-formation eruption,

Changbaishan, Northeast China, Lithos, 96, 315-324.

75. Wei, H., G. Liu, and J. Gill (2013), Review of eruptive activity at Tianchi volcano, Changbaishan, northeast China: implications for possible future eruptions, Bulletin of Volcanology, 75, 706, DOI 10.1007/s00445-013-0706-5.
76. Windley, B.F., Maruyama, S., Xiao, W.J., 2010. Delamination/thinning of sub-continental lithospheric mantle under Eastern China: the role of water and multiple subduction. Am. J. Sci. 310, 1250–1293.
77. Xu, Y., Li, H., Hong, L., Ma, L., Ma, Q., Sun, M., 2018. Generation of Cenozoic intraplate basalts in the big mantle wedge under eastern Asia. Science China Earth Sciences 61, 869-886.
78. Yang, J., Zhao, L., Kaus, B.J.P., Lu, G., Wang, K., Zhu, R., 2017. Slab-triggered wet upwellings produce large volumes of melt: insights into the destruction of the North China Craton. Tectonophysics. (in press).
79. Zhao, D., J. Lei, and R. Tang (2004), Origin of the Changbai intraplate volcanism in Northeast China: Evidence from seismic tomography, Chinese Science Bulletin, 49, 1401-1408.
80. Zhao, D., Ohtani, E., 2009. Deep slab subduction and dehydration and their geodynamic consequences: Evidence from seismology and mineral physics. Gondwana Res. 16, 401-413.
81. Zhao, D., Tian, Y., Lei, J., Liu, L., Zheng, S., 2009. Seismic image and origin of the Changbai intraplate volcano in East Asia: role of big mantle wedge above the stagnant Pacific slab. Phys. Earth Planet. Inter.173, 197–206.
82. Zhou, X., Armstrong, R., 1982. Cenozoic volcanic-rocks of eastern china- secular and

geographic trends in chemistry and strontium isotopic composition. Earth Planet. Sci. Lett. 58 (3), 301–329.

83. Zou, H., Fan, Q., Yao, Y., 2008. U–Th systematics of dispersed young volcanoes in NE China: Asthenosphere upwelling caused by piling up and upward thickening of stagnant Pacific slab. Chem. Geol. 255, 134–142.

Figures

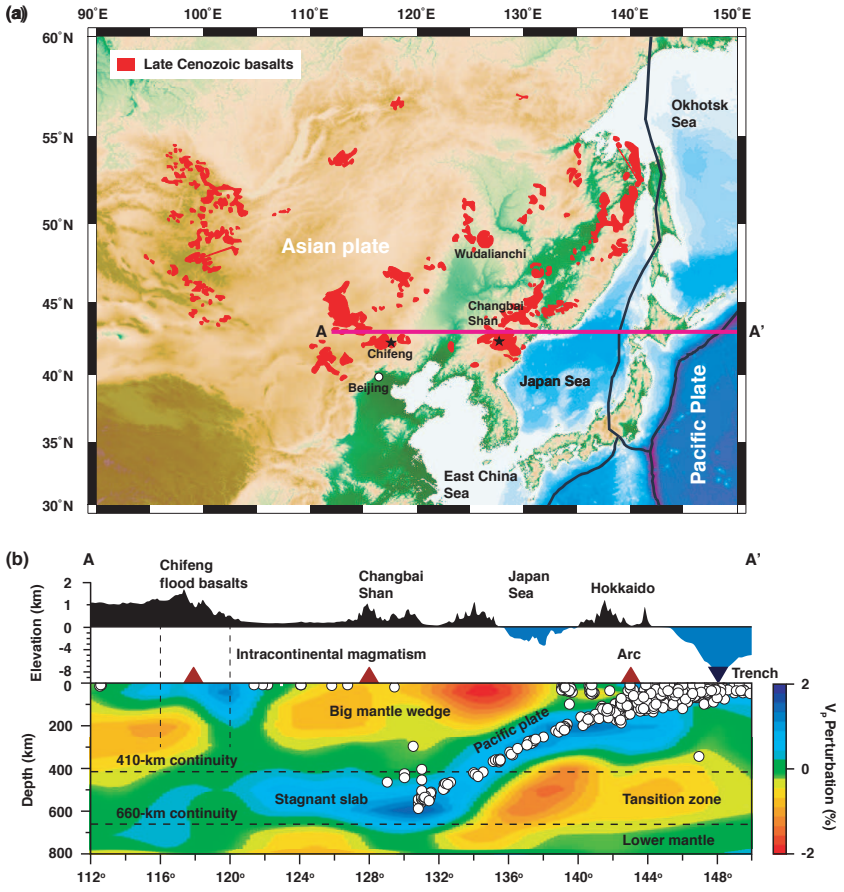

Figure 1. Distribution of the Cenozoic intracontinental volcanism in East Asia and stagnant slab in the TZ. (a) Topography map showing the distribution of the Cenozoic intraplate volcanism in East Asia. The red color indicates the location of the Cenozoic basalts, which are derived from [*Wang et al.*, 2015]. (b) A seismic tomography image showing the big mantle wedge and stagnant slab in the TZ beneath Northeast China (modified after [*Huang and Zhao*, 2006]).

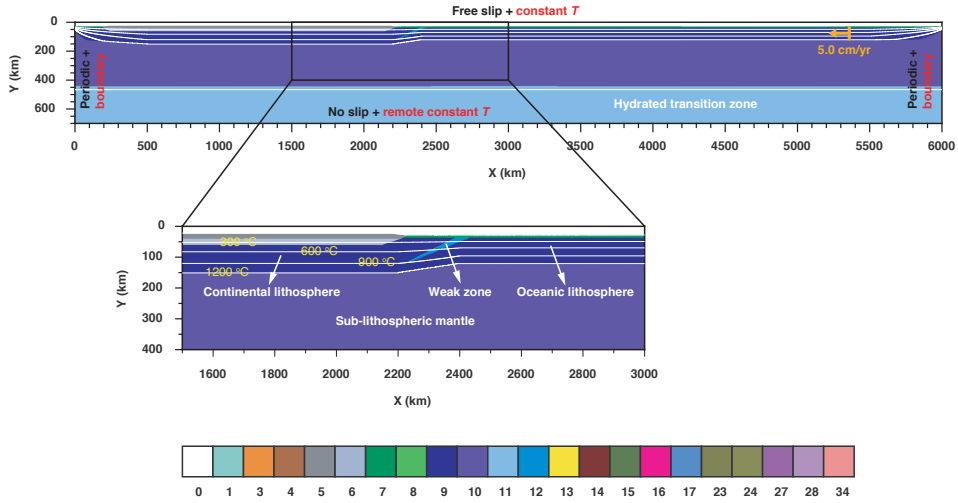

Figure 2. Model setup and boundary conditions. The upper panel (a) shows the whole model domain and boundary conditions. The lower panel (b) shows the zoomed-in configuration at the convergent margin. White lines overprinted on the composition fields show isotherms with an interval of 300 °C (the same below). The composition codes are shown at the bottom, with: 0, sticky air; 1, sea water; 3 and 4, sediment; 5, upper continental crust; 6, lower continental crust; 7, upper oceanic crust; 8, lower oceanic crust; 9, lithospheric mantle; 10, asthenospheric mantle; 11, hydrated mantle; 12, weak zone; 13, serpentinized mantle; 14, recrystallized (previously partially molten) mantle; 15, lower mantle; 16, extracted molten basalt; 17, extracted molten sediment or

upper continental crust; 23-24, partially molten sediment; 27, partially molten basalt; 28, partially molten gabbro; 34, partially molten wet peridotite

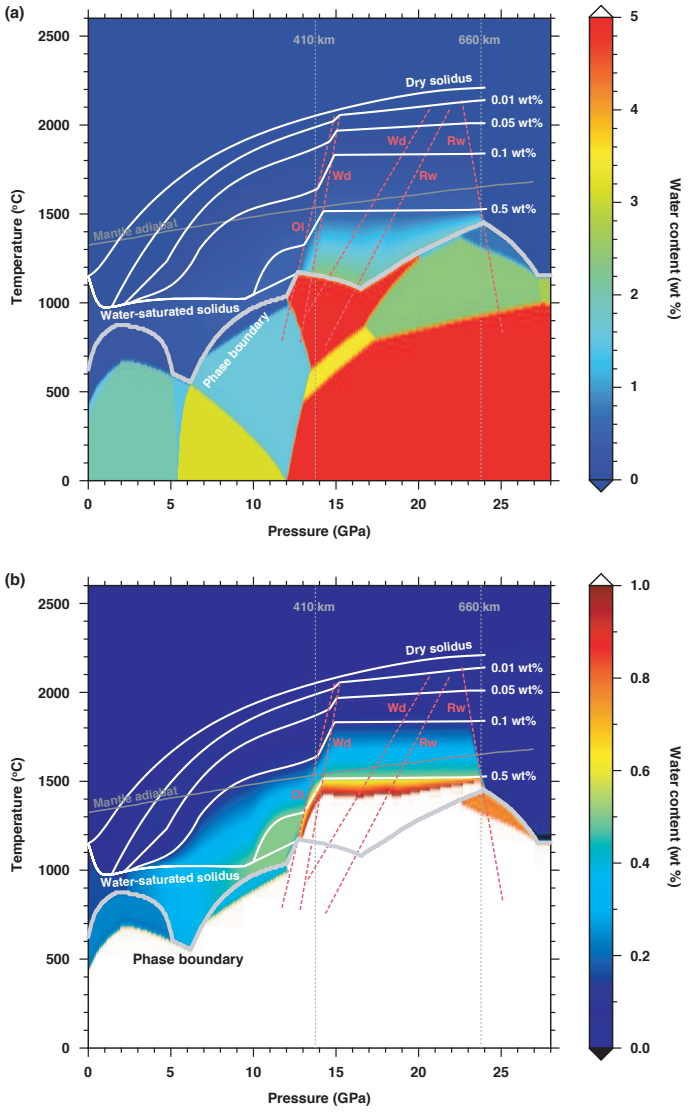

Figure 3. Phase relations and water contents of peridotite under hydrous conditions, modified after [*Iwamori*, 2004]. The white curves are solidi of peridotite with different water contents, compiled from the experimental results in [*Litasov*, 2011]. The water content in hydrous phases are taken from [*Iwamori*, 2004] and downscaled by about 3 times (see text). The maximum temperature at which hydrous phases are stable is indicated by the thick grey line. Water contents in NAMs (i.e., for temperature beyond the thick grey line) are taken from the wet solidi [*Litasov*, 2011] and

linearly interpolated for intermediate temperatures. In b) we show only water contents ≤ 1.0 wt% to better highlight the decreasing hydrogen solubility of NAMs as a function of the increasing P-T conditions in the upper mantle and transition zone. The dashed red lines indicate the main phase transitions and the gray line indicates the mantle adiabat [*Litasov et al.*, 2014]. Ol, olivine; Wd, wadsleyite; Rw, ringwoodite.

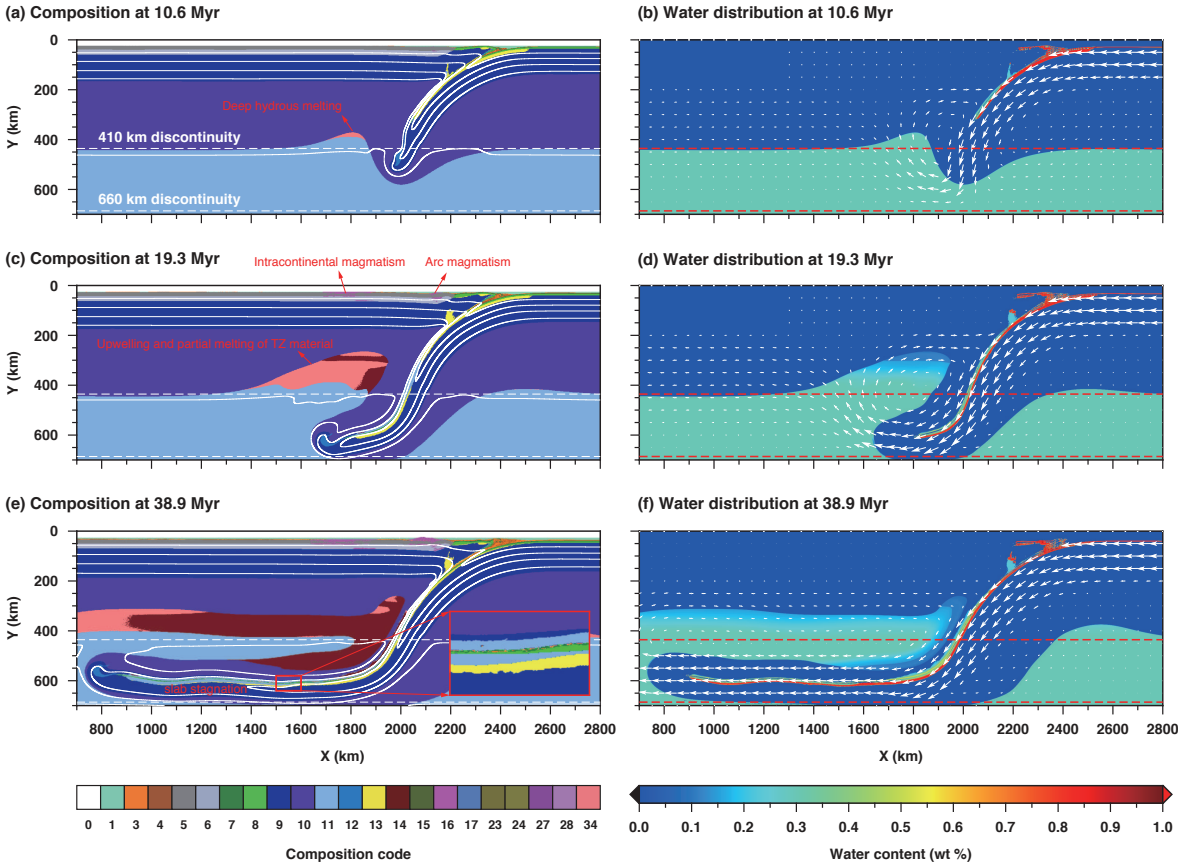

Figure 4. Time evolution of the reference model with 0.3 wt% water in the TZ ('Sta3' in Table 1). The left column shows the temporal evolution of the compositional field, while the right column shows the corresponding evolution of the water distribution. White arrows indicate the motion of the material. Dashed lines outline the unperturbed TZ. Color codes and isotherms as in Fig. 2.

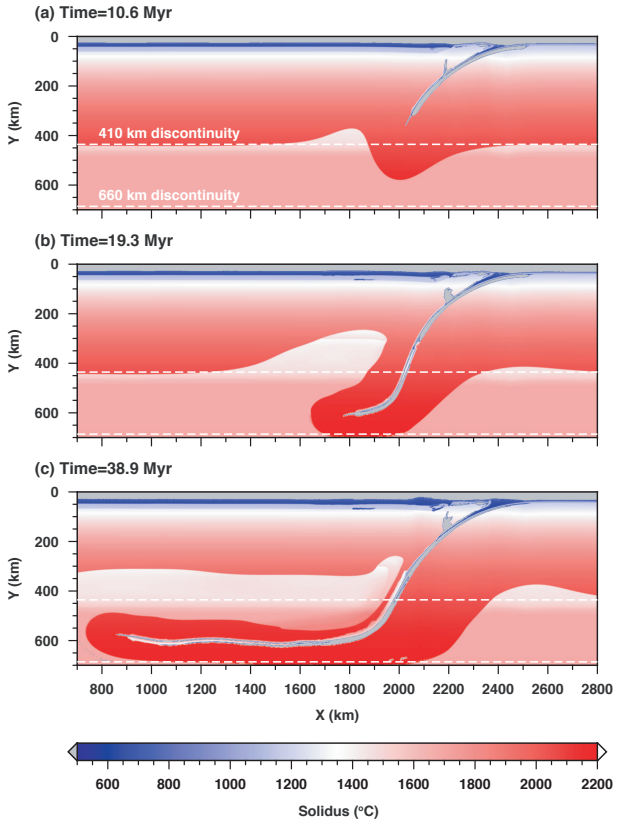

Figure 5. Snapshots of solidus temperature for the reference model with 0.3 wt% in the TZ. In grey material for which it is not possible to define a melting temperature (air, water, serpentinized rocks).

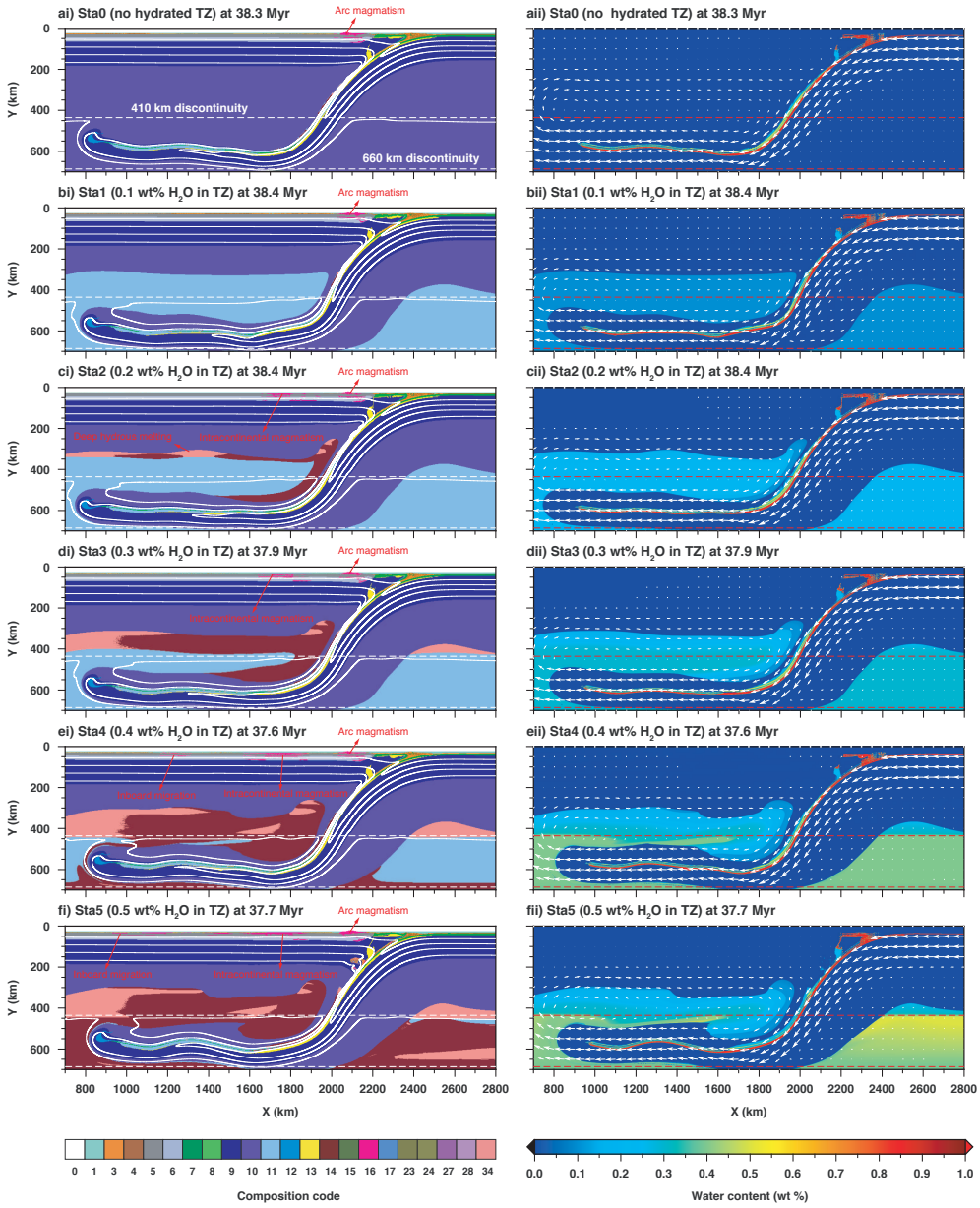

Figure 6. Comparison among the models with different water contents in the TZ. The left column (**i**) shows the snapshots of the compositional field resulted from the models with **(a)** an anhydrous TZ ('Sta0'), (**b**) a 0.1 wt% hydrous TZ ('Sta1'), (**c**) a 0.2 wt% hydrous TZ ('Sta2'), (**d**) a 0.3 wt% hydrous TZ ('Sta3'), (**e**) a 0.4 wt% hydrous TZ ('Sta4') and (**f**) a 0.5 wt% hydrous TZ ('Sta5'), while the right column (**ii**) shows the corresponding snapshots of the water distribution.

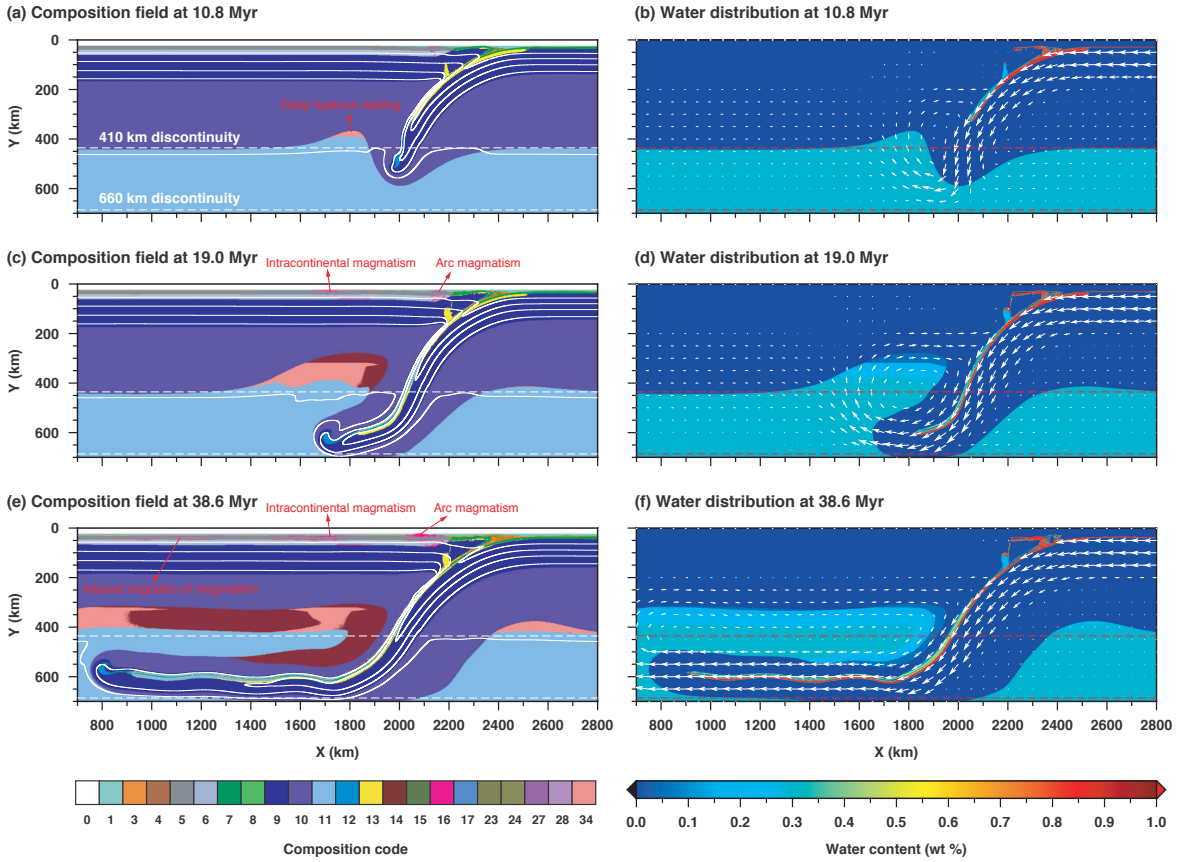

Figure 7. Time evolution of the model 'Sta6' (Table 1). This model is identical to the reference model except that it has a smaller minimum threshold of melt fraction for melt extraction ($\mathbf{M_{min}} = 1\%$). The left column shows the temporal evolution of the compositional field, while the right column shows the corresponding evolution of the water distribution. White arrows indicate the motion of the material. Dashed lines outline the unperturbed TZ.

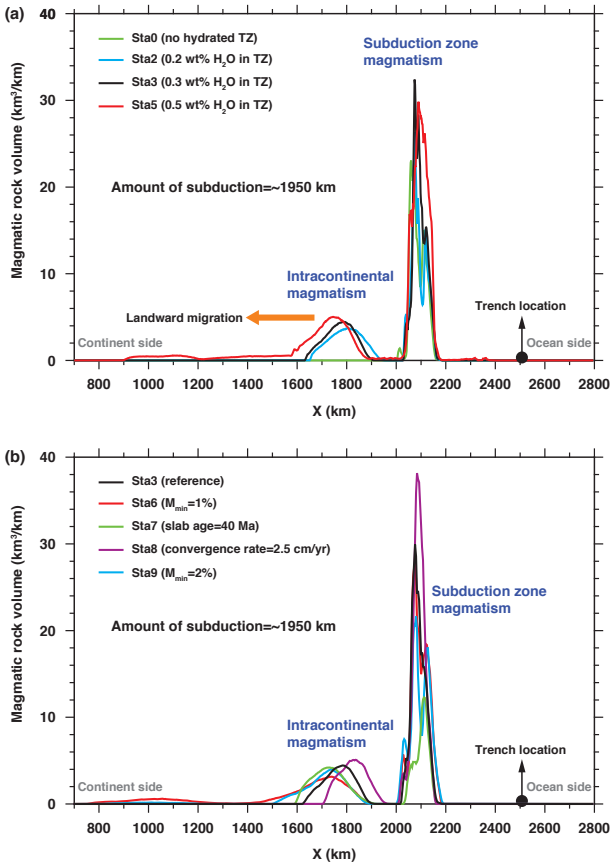

Figure 8. Volume of magmatic rocks resulted from different models. All the models are compared after the equivalent amount of subduction (~1950 km). The black arrow shows the position of the trench, and the orange arrow indicates the direction of intracontinental magmatism migration as the water content in the TZ increases.

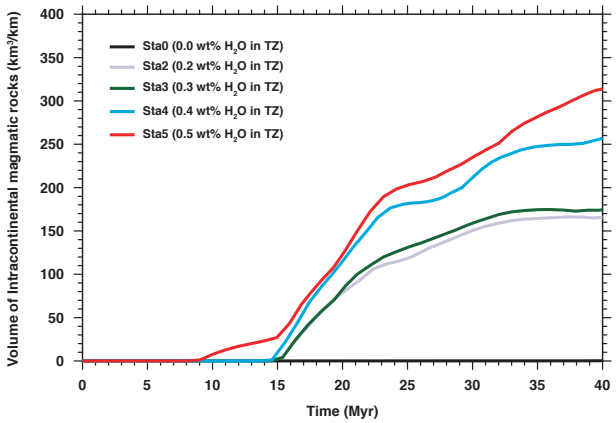

Figure 9. Evolution of intracontinental magmatism through time. The cumulative magmatic volumes are only counted for the region ranging from $0 \leq x \leq 2000\ km$ (i.e., intracontinental magmatism; see Figure 8). The arc magmatic rocks are not considered here.